14B.2 Relative humidity as a proxy for cloud formation over heterogeneous land surfaces

Chiel C. van Heerwaarden and Jordi Vilà-Guerau de Arellano
Meteorology and Air Quality Section, Wageningen University, The Netherlands
e-mail: chiel.vanheerwaarden@wur.nl

1. Introduction [1]

Convective cloud formation over land is a complex phenomenon due to the strong interaction between the land surface and the atmospheric boundary layer (ABL) (Kang et al., 2007). Previous studies (e.g. Ek and Mahrt, 1994; Ek and Holtslag, 2004) described the underlying physics of these interactions over homogeneous land surfaces. However, it has been suggested (e.g. Crook, 1997; Pielke, 2001; Kang et al., 2007) that the timing and location of cloud formation are sensitive to heterogeneous forcings at the land surface, which depend on the spatial variability of land use, soil moisture content and topography.

Heterogeneous forcings occur over a wide range of scale levels, but the strongest effects on ABL properties are found when the heterogeneities are in the meso-γ scale (2-20 km) (Mahrt, 2000), since they modify the horizontal and vertical structure of the ABL by inducing circulations. A consequence is that the effects of heterogeneity-induced circulations are difficult to be represented well by mesoscale and large-scale models, as these flows are mostly in the subgrid scales of the models. To date we lack adequate parameterizations, because the effects of circulations on cloud formation in the meso-γ scale are not fully understood.

By using an LES model, we studied the spatial distribution of entrainment and compared the total entrainment for cases with varying heterogeneity amplitudes and inversion strengths for potential temperature and specific humidity. By applying a statistical decomposition between turbulent and mesoscale components, we investigate the contribution of the heterogeneity-induced circulation to entrainment. Later, we connect our findings about the ABL height and entrainment processes to the thermodynamic changes in the ABL by studying the specific humidity and the RH. We analyzed the spatial structure of temperature, moisture and RH near the top of the ABL for different heterogeneity amplitudes and inversion strengths of potential temperature and specific humidity. Vertical profiles of the RH and the variances of potential temperature and specific humidity were analyzed in order to study the modification of the horizontally averaged profiles by heterogeneous forcings.

2. Numerical methods

2.1 *Model description*

The study is based on numerical experiments performed using the Dutch Atmospheric LES (DALES) model, which was initially developed by Nieuwstadt and Brost (1986), improved by Cuijpers and Duynkerke (1993) and updated to a parallel-processing version by Dosio et al. (2005). DALES solves the filtered Navier-Stokes equations with the Boussinesq approximation applied.

DALES has periodic boundary conditions in the horizontal plane. At the land surface the surface fluxes for heat $\overline{w'\theta'}$ and moisture $\overline{w'q'}$ and the friction velocity u_* are prescribed. There is a sponge layer in the top of the model, which prevents the reflection of gravity waves back into the model domain.

2.2 *Experimental setup*

For this study we discretized our LES-domain into 256 x 192 x 192 grid cells on the x, y and z axes. The grid length is 25 m in x and y and 12.5 m in z and our domain is thus 6400 x 4800 x 2400 m. All cases are dry convective boundary layers with prescribed surface heat fluxes. There is no background wind ($U_g = V_g = 0$ m s^{-1}) and the friction velocity u_* is fixed at 0 m s^{-1} i.e. free local convection. The initial profiles and surface forcings correspond to the temperature and moisture conditions of a typical early summer day in The Netherlands. All simulations have an initial potential temperature profile that is constant with height for the first 800 m. On top of this layer we prescribe a temperature jump (case dependent) and after this jump the stratified free atmosphere has a temperature lapse rate equal to 0.006 K m^{-1}. The initial specific humidity profile in the mixed layer is constant with height (0.005 kg kg^{-1}), with a jump on top of the mixed layer and a constant value in the free atmosphere (case dependent). The selected value for the potential temperature jump ($\Delta\theta$) determines the growth rate of the ABL. In case of a small jump, the ABL grows fast and and due to the pressure decrease at the top, the ABL top cools in terms of absolute temperature, which has a positive effect on the RH$_{zi}$. On the other hand, if the jump is small, a large amount of free atmospheric air enters the ABL. For this air the specific humidity jump (Δq) determines the dryness and thus in what extent the cooling can be compensated by drying.

In order to create heterogeneous forcings, the land surface is divided in two parts along the x-axis. All grid cells in the left patch (cells 1 to 128) are characterized by a Bowen ratio below the average Bowen ratio (the cold patch) and the cells in the right patch (grid cell 129 to 256) have an above average Bowen ratio (the warm patch). The length of the heterogeneity (one cycle of a cold and a warm patch) is therefore 6400 m. As the ABL heights vary between 1000 and 1100 m, the ratio between the heterogeneity length and the ABL height is in the range that AV98 and PA05 specify for the strongest

[1] This abstract is a summary of Van Heerwaarden and Vilà-Guerau de Arellano (2008). Further details can be found in this manuscript.

Table 1: Initial conditions for all LES simulations. θ_{ML} is the initial mixed layer potential temperature, $\Delta\theta$ is the temperature jump at 800 m, Δq is the temperature jump at 800 m.

simulation	θ_{ML} [K]	$\Delta\theta$ [K]	Δq [kg kg^{-1}]
$Case1$	293.0	2.0	0.000
$Case2$	293.0	2.0	0.000
$Case3$	293.0	2.0	0.000
$Case4$	293.0	2.0	0.000
$Case5$	293.0	2.0	0.000
$Weak1$	294.5	0.5	0.000
$Weak5$	294.5	0.5	0.000
$Case1dry$	293.0	2.0	-0.004
$Case5dry$	293.0	2.0	-0.004
$Weak1dry$	294.5	0.5	-0.004
$Weak5dry$	294.5	0.5	-0.004
$Case1large$	293.0	2.0	0.000
$Case5large$	293.0	2.0	0.000

mesoscale contribution to the flow.

We performed a sensitivity analysis on the heterogeneity amplitude, which is defined as the Bowen ratio difference between the cold and the warm patches. In all cases, for every location at the land surface, the sensible H and latent LE heat flux add up to 360 W m^{-2}, but the Bowen ratios for the cold and the warm patch differ among the simulations (see Table 2). For the three other regimes we simulated the homogeneous and the largest amplitude case.

All cases were initially integrated for three hours. After three hours of spin-up, the three components of the wind, the potential temperature and specific humidity were recorded for each grid cell every five seconds for one hour. The statistics are thus based on 720 time steps.

2.3 *Statistical methods*

To calculate the turbulent statistics of our model runs we used a method based on phase averaging (Hussain and Reynolds, 1970). A similar method was previously employed in the LES study of heterogeneous land surfaces by PA05. Our model forcings are heterogeneous only on the x-axis and thus homogeneous on the y-axis. Therefore, we assume that a local spatial average can be calculated by averaging over y. We decompose an arbitrary space- and time-dependent turbulent variable $\phi_{x,y,z,t}$ in two components.

$$\phi_{x,y,z,t} = \langle\phi\rangle_{x,z,t} + \phi'_{x,y,z,t} \quad (1)$$

We name the first term on the right hand side the local average, which is the spatial average of all values on the y-axis that share the same x, z and t-coordinates. Under homogeneous conditions $\langle\phi\rangle_{x,z,t}$ equals the slab average as there are no variations in local spatial averages in a horizontal plane. The difference between the local average and the slab average is thus a measure of advection and therefore of the contribution of the heterogeneous surface forcings to the statistics. This contribution we call the meso scale component from now on. The turbulent fluctuation $\phi'_{x,y,z,t}$ is the second term. In the further analyses we denote spatial averages in the y-direction as $\langle\phi\rangle$ and in the x-direction as $[\phi]$. Temporal averages are denoted as $\overline{\phi}$.

3. Results

3.1 *Entrainment processes and ABL growth*

3.1.1 Structure of the ABL top and entrainment

Our first objective was to study the influence of the heterogeneity amplitude on entrainment processes and on the evolution of the ABL height. Figure 1 shows the 1-h averaged ABL height as a function of space along the x-axis. The heights are derived using the maximum potential temperature gradient following the procedure in Sullivan et al. (1998). For every x, y-coordinate the ABL height is calculated for each time step and these values are averaged over y and time. The values in the figure are scaled by the horizontally averaged ABL height.

Figure 1 shows that the presence of horizontal variability in the surface forcings results in a spatial variability of the ABL height z_i along the heterogeneity. The homogeneous case ($Case1$) has an ABL height that is $z/z_i = 1.0$ with small fluctuations around this value, whereas in all heterogeneous cases a clear spatial pattern is visible, with a deeper boundary layer over the warm patch. Therefore, we corroborate the earlier findings of AV98 and PA05 who showed ABL height variations for different heterogeneity lengths.

Slight variations in this pattern are visible, caused by differences in the heterogeneity amplitude. For instance, above the warm patch (x/λ = 0.5), there is an increase in ABL height related to the larger heterogeneity amplitude. $Case2$ has a height that is 4 per cent larger than the average ABL height ($z/z_i = 1.04$), whereas $Case5$ attains values up to 5 per cent larger ($z/z_i = 1.05$) than the average. Over the cold patch, the opposite effect is visible, with a decreasing ABL height for increasing heterogeneity amplitude. In spite of the small variations caused by the heterogeneity amplitude, the main variations in ABL height are due solely to the presence of a heterogeneity-induced circulation. For cases with weak inversions (not shown), we found for $Case5dry$ the same relative increase over the warm patch ($z/z_i = 1.05$).

Figure 2 shows the spatial distribution of entrainment and contains the cross sections of the 1-h averaged values of the normalized turbulent heat flux $\overline{\langle w'\theta'_v\rangle} / \left[\overline{\langle w'\theta'_v\rangle}_0\right]$ for $Case2$ and $Case5$. The overlying vector plot shows the wind that is driven by the differential heating of the domain. Before analyzing the figure, it is worth mentioning that the average subgrid scale contribution to the heat flux at z/z_i = 0.95 is 5.6 % for $Case5$ (subgrid flux 0.0011 K m s^{-1}, resolved 0.0183 K m s^{-1}), which indicates that the resolved part largely exceeds the subgrid part, thus that the flow is resolved accurately.

A stronger heterogeneity amplitude results in stronger surface winds towards the center of the warm

Table 2: Surface boundary conditions for all LES simulations. H_L is the sensible heat flux of the cold patch, H_R is the sensible heat flux of the warm patch, LE_L is the latent heat flux of the cold patch, LE_R is the latent heat flux of the warm patch, β_L is the Bowen ratio of the cold patch, β_R is the Bowen ratio of the warm patch.

simulation	H_L [W m^{-2}]	H_R [W m^{-2}]	LE_L [W m^{-2}]	LE_R [W m^{-2}]	β_L [-]	β_R [-]
$Case1$	120	120	240	240	0.50	0.50
$Case2$	105	135	255	225	0.41	0.60
$Case3$	90	150	270	210	0.33	0.71
$Case4$	75	165	285	195	0.26	0.85
$Case5$	60	180	300	180	0.20	1.00
$Weak1$	120	120	240	240	0.50	0.50
$Weak5$	60	180	300	180	0.20	1.00
$Case1dry$	120	120	240	240	0.50	0.50
$Case5dry$	60	180	300	180	0.20	1.00
$Weak1dry$	120	120	240	240	0.50	0.50
$Weak5dry$	60	180	300	180	0.20	1.00
$Case1large$	120	120	240	240	0.50	0.50
$Case5large$	60	180	300	180	0.20	1.00

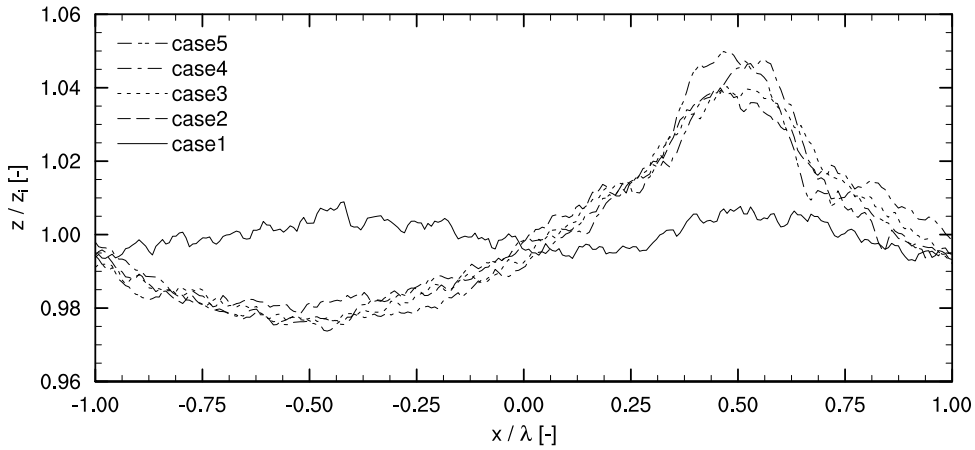

FIG. 1: Averaged ABL height along the x-coordinate during 1 h. Horizontal coordinates are scaled by the patch size λ, vertical coordinates are scaled by the time- and area-averaged ABL height $\left[\overline{\langle z_i \rangle}\right]$.

patch where thermals are merged. $Case2$ has, for instance, a wind of approximately 1 m s^{-1} at $x/\lambda = 0.3$ and $z/z_i = 0.05$, whereas $Case5$ has more than 2 m s^{-1} at the same location. The strongly buoyant thermals that are the product of the merging can penetrate the entrainment zone more vigorously, thereby locally enhancing entrainment, for instance at $x/\lambda = 0.5$ and $z/z_i = 1.0$. The normalized entrainment minima found for $Case2$ are -0.4 and -0.6 times the surface flux, while in $Case5$ the values have a range from -0.8 to -1.0 times the surface flux. These local values largely exceed the ratio of -0.2 times the surface flux that is widely used in parameterizations of the entrainment flux. Although the ABL heights over the warm patch are only slightly sensitive to heterogeneity amplitude, the entrainment minima increase greatly with increasing amplitude. In the next section we discuss the effects of this local entrainment enhancement on the total area averaged entrainment over the heterogeneous land surfaces.

In contrast to the warm patch, over the cold patch thermals are surpressed by the downward wind of the induced mesoscale circulation (downward motions x/λ = -1.0 to 0.0). At the top of the ABL winds are directed towards the cold patch (x/λ = 0.2 and 0.8). Convergence of air occurs here and the warm air is advected downwards towards the land surface. This downward-moving warm air does not allow thermals generated over the cold patch to reach the ABL top and thereby prevents entrainment over the cold patch. The line at which the turbulent flux becomes zero is located at z/z_i = 0.7 for $Case2$ and at z/z_i = 0.5 for $Case5$. The surpression of upward moving thermals is thus enhanced as heterogeneity amplitude increases. Above the warm patch we find strong upward motions (more than 3 m s^{-1} for $Case5$) over a small area, while the cold patch has gentle downward motions (less than 1 m s^{-1}) over the whole cold patch.

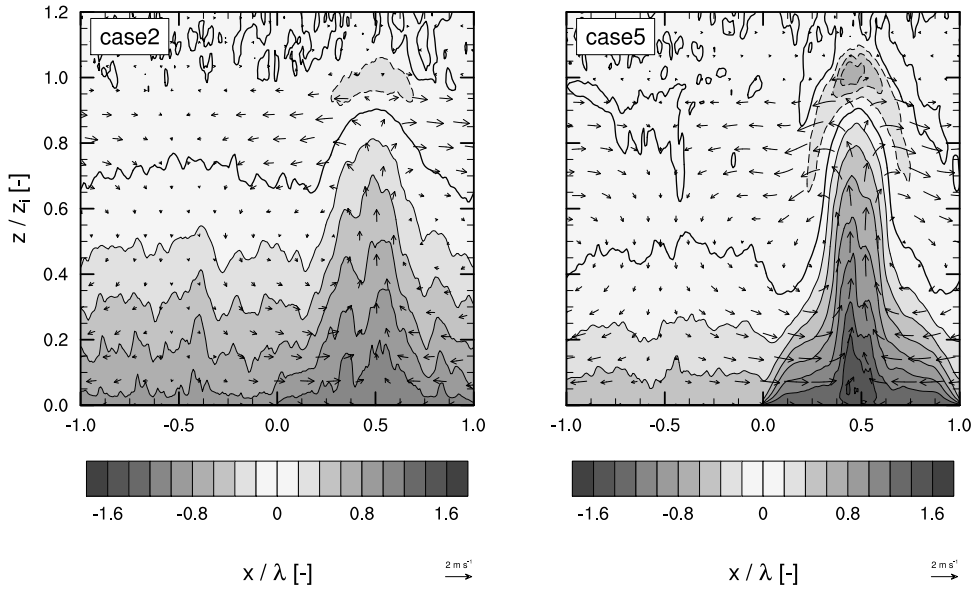

FIG. 2: Cross-section of the 1-h-averaged normalized turbulent heat transport $\overline{\langle w'\theta'_v \rangle} / \left[\overline{\langle w'\theta'_v \rangle}_0\right]$ for $Case2$ (left) and $Case5$ (right). Vectors indicate the wind direction and magnitude. The horizontal coordinates are scaled by the patch size λ and the vertical coordinates are scaled by the ABL height $\left[\langle z_i \rangle\right]$.

3.1.2 AREA AVERAGED ABL GROWTH AND ENTRAINMENT

Here, we further discuss the effects of surface variability on the thermodynamic vertical profiles. To address these effects, the vertical profiles of the homogeneous $Case1$ are compared with the four heterogeneous cases. Just as a reminder, notice that all cases have the same area-averaged sensible and latent heat flux and initial thermodynamic profiles. Consequently, differences among the simulations must be induced by the heterogeneous forcings and by the subsequent local effects on entrainment.

Figure 3 shows the 1-h area averaged heat flux profiles for all the simulations. In spite of the large structural changes that heterogeneity induces, there are only small differences between the homogeneous and heterogeneous cases, although as we show later, the distribution between mesoscale and turbulent contributions to the heat flux varies considerably. All cases show a linear heat flux profile in the ABL (z/z_i = 0 - 0.8) and an area of negative heat flux at the top of the ABL which is characterizing the entrainment zone (z/z_i = 0.8 - 1.1). The curved profiles of the heat flux that AV98 found for heterogeneous cases are not present in our cases. We found linear profiles similar to those in PA05. Therefore, we assume that heterogeneous cases should yield linear profiles and that AV98 results are the effect of the low resolution of their model runs.

Figure 4 shows the temporal evolution of the area-averaged ABL height for all five cases computed following the maximum temperature gradient method (Sullivan et al., 1998). After three hours of spin-up, the ABL heights of $Case4$ (1000 m) and $Case5$ (1010 m) are the largest, but the growth rate of all five cases, which is

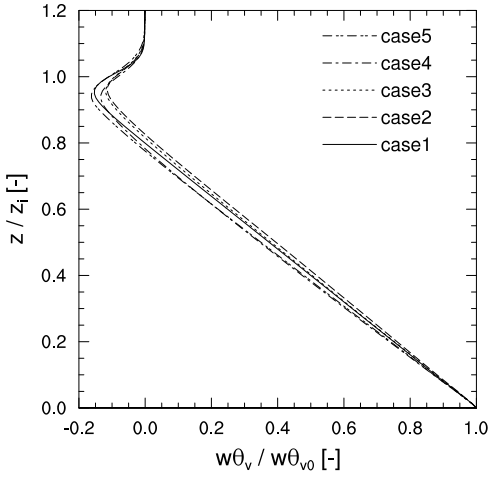

FIG. 3: Vertical profiles of the 1-h-averaged total heat transport $\left[\overline{w\theta_v}\right]$. Horizontal coordinates are scaled by the surface sensible heat flux $\left[\overline{\langle w'\theta'_v \rangle}_0\right]$, vertical coordinates are scaled by the ABL height $\left[\langle z_i \rangle\right]$.

the entrainment velocity, has a similar magnitude (approximately 70 m h^{-1}). If all cases have the same entrainment velocity, the entrainment differences found in the previous section can not exist. Therefore, the suggested enhancement found in Figure 3 may be the result of the horizontal averaging, where the strongest amplitude cases have a deeper negative area due to the greater variability in ABL height over the domain. This connects with the findings of Lilly (2002) who suggest that the smooth heat flux profiles in the entrain-

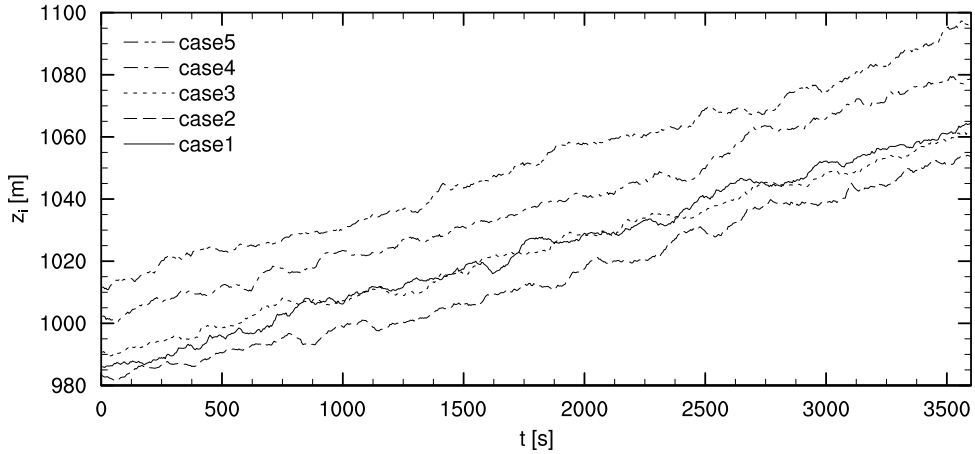

FIG. 4: Domain-averaged ABL height $[\langle z_i \rangle]$ during the hour of data recording.

ment zone found in LES are mostly an effect of horizontal averaging and the that link to the entrainment rate should be made carefuly. PA05 found no significant enhancement of entrainment when they performed a sensitivity analysis of the effect of the heterogeneity length, but they did not vary the heterogeneity amplitude. We showed by varying the amplitude that the results of PA05 are correct and we thus disagree on previous suggestions of AV98 and Letzel and Raasch (2003) that the area averaged entrainment is enhanced.

3.2 *Relative humidity in the ABL*

3.2.1 SPATIAL DISTRIBUTION OF RELATIVE HUMIDITY

Relative humidity is the indicator that links the results of the boundary layer growth and temperature analyses with the findings on the moisture structure. Here, we include the simulations that are performed for the regimes with weaker temperature inversions and a drier upper atmosphere to investigate the importance of the thermodynamic structure of the entrainment zone. Figure 5 shows the 1-h-averaged cross-section of $\overline{\langle RH \rangle}$ for $Case5dry$. The ABL top over the warm patch reaches values up to RH = 55 % (x/λ = 0.5, z/z_i = 0.95), while the cold patch does not exceed RH = 30 %. At the center of the cold patch, there is a dry area at x/λ = -0.5, z/z_i = 0.9 caused by the entrained dry air that is transported downwards here (see vectors in Figure 5). Above the center of the cold patch (x/λ = 0.5), the RH is the minimum for that height. The effects of dry air entrainment extend down to the land surface, as the surface RH at x/λ = -0.5 is less than 30 per cent, while over the warm patch at x/λ = 0.5, the RH exceeds 35 per cent.

The maximum RH over the warm patch (RH = 62.5 %) of $Case5$ exceeds the value found over a homogeneous land surface sharing the same area-averaged fluxes (RH = 59 %, see Figure 7). In the cases characterized by a drier upper atmosphere, the RH-enhancement effect is still important, despite the intense dry air entrainment, since this air is horizontally

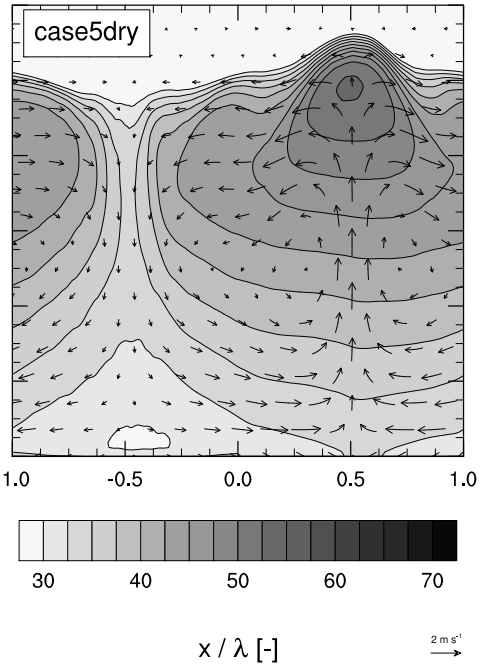

FIG. 5: Cross section of the 1-h-averaged relative humidity $\overline{\langle RH \rangle}$ for $Case5dry$. The horizontal coordinates are scaled by the patch size λ and the vertical coordinates are scaled by the ABL height z_i. Vectors indicate the wind direction and magnitude.

advected towards the cold patch and does not directly influence the RH over the center of the warm patch (see Figure 5). As RH is our chosen indicator for cloud formation (Ek and Mahrt, 1994), we therefore expect that in free convective conditions cloud formation may occur earlier over heterogeneous land, independent of temperature and moisture inversion strengths. This finding provides a more complete explanation of previous studies (Avissar and Liu, 1996) that found that cloud formation is enhanced over areas that are warmer and drier

than their environment.

3.2.2 VARIABILITY OF AREA AVERAGED RELATIVE HUMIDITY

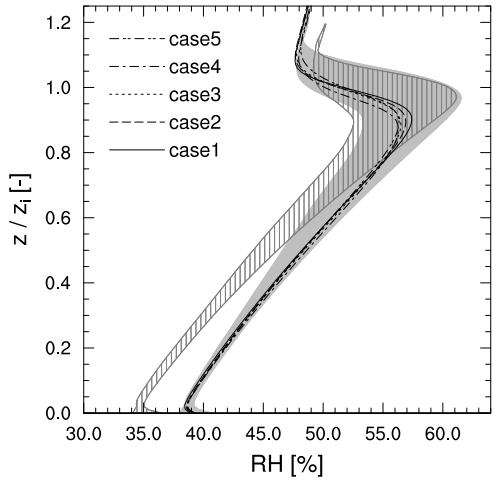

FIG. 6: Vertical profile of the spatial- and time-averaged value of the relative humidity $\overline{\langle RH \rangle}$ for all cases (left). The gray shading shows the range of time-averaged values of relative humidity $\overline{\langle RH \rangle}$ within the domain of $Case5$. The gray hatched area shows the same range but for $Weak5$.

Figure 6 shows the 1-h-averaged vertical profiles of the relative humidity. In the left figure, the shaded area is the range of the 1-h-average relative humidities found in $Case5$, the hatched area is the range of temporal averaged RHs in $Weak5$. This figure shows that the mean profiles of RH are nearly identical, with the maximum RH at $z/z_i = 0.95$. The large-amplitude cases are characterized by a deeper entrainment zone (see Figure 3), which tend to distribute the moisture over a larger region. The RH peak in the homogeneous case is thus slightly higher (RH = 57 %) than in the heterogeneous cases (RH = 55 %). Notice that the area averaged RH is not enhanced by heterogeneity, which is supported by the fact that we have identical surface fluxes and entrainment velocities for all amplitudes (see Figure 4).

The large RH-variability of $Case5$ (grey shaded area) indicates the importance of variability on possible cloud formation. The mean profiles of $Case1$ and $Case5$ are very similar, but in $Case1$ there is hardly any variability within the domain (not shown). In $Case5$ we find a range of 7 % (RH = 54 - 61 %) within the domain. This variability range is even larger (9 %, RH = 52 - 61 %) if the temperature inversion strength becomes weaker, caused by the extra dry air entrainment that sinks over the cold patch.

Figure 7 shows the maximum time-averaged $\overline{\langle RH \rangle}$ found in the entrainment zone for all cases. The maximum value of RH increases with heterogeneity amplitude for the four defined regimes of potential temperature and specific humidity inversion strengths. For the numerical experiments with a strong inversion, the values range from 59.4 % ($Case1$) to 61.8 % ($Case5$) for a moist upper atmosphere and from 48.5 % ($Case1dry$) to 51.0 % ($Case5dry$) in the dry case. The weak inversion cases show a slightly stronger correlation between the maximum RH and the heterogeneity amplitude ($Weak1$ = 57.4 %, $Weak5$ = 61.3 %, $Weak1dry$ = 43.0 %, $Weak5dry$ = 47.0 %), which is in agreement with our previous finding that in weak inversions the ABL height variability is relatively larger compared to the strong inversion cases. Although a difference of 3 - 4 % between the homogeneous and strongest heterogeneous case is small, Ek and Mahrt (1994) found that in the afternoon the typical RH$_{zi}$ tendency per hour has similar values. Therefore, there might be a difference in cloud onset between the homogeneous and heterogeneous cases in the order of an hour, if we would take initial conditions for the LES simulations closer to saturation.

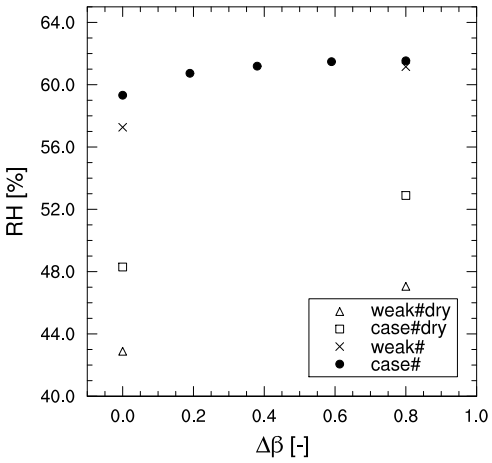

FIG. 7: Relation between the maximum time averaged relative humidity $\overline{\langle RH \rangle}_{max}$ per domain versus the heterogeneity amplitude, $\Delta\beta$ for all regimes. The # can be substituted by the number of the case.

4. Summary and conclusions

We investigated the effect of heterogeneous forcings on the potential formation of convective clouds using relative humidity as an indicator. This was done by analyzing numerical experiments using a large eddy simulation model. A sensitivity analysis was performed on the heterogeneity amplitude and the inversion strengths of potential temperature and specific humidity for a land surface that is heterogeneous in the meso-γ scale (2 - 20 km). The cases are integrated for four hours of which the last hour was used to record statistics. We analyzed the height of the ABL, the specific and relative humidity structure near the ABL top for a free convective boundary layer that was forced by a sensible and latent heat flux that added up to 360 W m^{-2} for all simulations. The land surface was divided in 2 patches, one with a low Bowen ratio (cold patch) and one with a high Bowen ratio (warm patch). Different heterogeneity amplitudes were simulated by varying the difference between the

Bowen ratios of the two patches.

An analysis of entrainment and ABL growth of the heterogeneously forced ABL indicated that under heterogeneous conditions the ABL increases over the warm patch, and decreases over the cold patch. The greater ABL heights over the warm patch lead to lower absolute temperatures over the center of the warm patch. Due to the mesoscale circulation that is induced by the heterogeneous forcings, moisture is advected to the center of the warm patch. Low absolute temperatures in combination with high specific humidity over the warm patch lead to a situation which has a relative humidity that is higher under heterogeneous condititions than under homogeneous forcings. These are the first indications in this study that cloud formation may be favorable over the warm patches of a heterogeneous landscape.

The comparison of vertical heat flux profiles of homogeneous and heterogeneous cases sharing the same area-averaged forcings revealed that entrainment in low-amplitude heterogeneous cases appears to be less than in homogeneous cases, whereas the entrainment of large amplitude cases exceeds the entrainment of homogeneous cases. Nevertheless, this finding is rejected by the analysis of the time evolution of the ABL height, as identical entrainment velocities for all cases are found here.

Mean vertical profiles of relative humidity are very similar in all cases, but the variability in the time-averaged RH near the top of the ABL (RH_{zi}) is largely enhanced by the presence of heterogeneity. This finding is proven to be true for all cases with strong and weak potential temperature inversions and with moist and dry upper atmospheres. In all situations the RH_{zi} over the warm patch is larger than over the cold patch and than in homogeneous conditions. By conditionally sampling the data, we show that thermals over heterogeneous surface conditions are more effective in transporting moisture upwards, due to their larger volume to surface ratio. In addition, the RH cross sections show that dry air that is entrained is transported downwards mostly over the cold patch and low values of RH are found over this patch. In cases with a drier free atmospheres, these effects can be more pronounced and dry entrainment events extend to the land surface. Therefore, we conclude that the mean RH profile shows incomplete information with regard to RH modifications by heterogeneity. It is highly relevant to calculate the variability of RH as a function of the amplitude of the heterogeneity, as this variable contains the influence of heterogeneity on the maximum RH that occurs in the domain.

All of the above findings suggest that land surface heterogeneity plays a significant role in the stucture and value of the RH_{zi}. Cloud formation may be enhanced over heterogeneous landscapes as the maximum RH and the specific humidity variance in the entrainment zone are larger than in homogeneous conditions.

Acknowledgments. The authors acknowledge the helpful comments of Ned Patton, Stephan de Roode and Joel Schröter. This study was supported by a grant from the Netherlands Organisation for Scientific Research (NWO TopTalent). This work was sponsored by the National Computing Facilities (NCF project SG132).

REFERENCES

Avissar, R. and Y. Liu, 1996: Three-dimensional numerical study of shallow convective clouds and precipitation induced by land surface forcing. *J. Geophys. Res.*, **101**, 7499–7518.

Crook, N. A., 1997: Sensitivity of moist convection forced by boundary layer processes to low-level thermodynamic fields. *Mon. Wea. Rev.*, **124**, 1767–1785.

Cuijpers, J. W. M. and P. G. Duynkerke, 1993: Large-eddy simulation of trade-wind cumulus clouds. *J. Atmos. Sci.*, **50**, 3894–3908.

Dosio, A., J. Vilà-Guerau de Arellano, A. A. M. Holtslag and P. J. H. Builtjes, 2005: Dispersion of a passive tracer in buoyancy- and shear-driven boundary layers. *J. Atmos. Sci.*, **42**, 1116–1130.

Ek, M. B. and A. A. M. Holtslag, 2004: Influence of soil moisture on boundary layer cloud development. *J. Hydrometeor.*, **5**, 86–99.

Ek, M. B. and L. Mahrt, 1994: Daytime evolution of relative humidity at the boundary layer top. *Mon. Wea. Rev.*, **122**, 2709–2721.

Hussain, A. K. M. F. and W. C. Reynolds, 1970: The mechanics of an organized wave in turbulent shear flows. *J. Fluid Mech.*, **41**, 241–258.

Kang, S.-L., K. J. Davis and M. LeMone, 2007: Observations of the abl structures over a heterogeneous land surface during ihop2002. *J. Hydrometeor.*, **8**, 221–244.

Letzel, M. O. and R. Raasch, 2003: Large eddy simulation of thermally induced oscillations in the convective boundary layer. *J. Atmos. Sci.*, **60**, 2328–2341.

Lilly, D. K., 2002: Entrainment into mixed layers. part i: Sharp-edged and smoothed tops. *J. Atmos. Sci.*, **59**, 3340–3352.

Mahrt, L., 2000: Surface heterogeneity and vertical structure of the boundary layer. *Bound.-Layer Meteor.*, **96**, 33–62.

Nieuwstadt, F. T. M. and R. A. Brost, 1986: The decay of convective turbulence. *J. Atmos. Sci.*, **43**, 532–546.

Pielke, R. A., 2001: Influence of the spatial distribution of vegetation and soils on the prediction of cumulus convective rainfall. *Rev. Geophys.*, **39**, 151–178.

Sullivan, P. P., C. H. Moeng, B. Stevens, D. Lenschow and S. D. Mayor, 1998: Structure of the entrainment zone capping the convective atmospheric boundary layer. *J. Atmos. Sci.*, **55**, 3042–3064.

van Heerwaarden, C. C. and J. Vilà-Guerau de Arellano, 2008: Relative humidity as an indicator for cloud formation over heterogeneous landscapes. *J. Atmos. Sci.*, **in press**.